ATR-FTIR Redox Difference Spectroscopy of *Yarrowia lipolytica* and Bovine Complex I†

Douglas Marshall,‡ Nicholas Fisher,‡ Ljuban Grigic,§ Volker Zickermann,§ Ulrich Brandt,§ Richard J. Shannon,|| Judy Hirst,|| Rebecca Lawrence,‡ and Peter R. Rich*,‡

Glynn Laboratory of Bioenergetics, Department of Biology, University College London, Gower Street, London WC1E 6BT, U.K., Zentrum der Biologischen Chemie, Fachbereich Medizin, Universität Frankfurt, D-60590 Frankfurt am Main, Germany, and Medical Research Council Dunn Human Nutrition Unit, Wellcome Trust/MRC Building, Hills Road, Cambridge CB2 2XY, U.K.

Received December 16, 2005; Revised Manuscript Received March 13, 2006

ABSTRACT: ATR-FTIR spectroscopy in combination with electrochemistry has been applied to the redox centers of *Yarrowia lipolytica* complex I. The redox spectra show broad similarities with previously published data on *Escherichia coli* complex I and with new data here on bovine complex I. The spectra are dominated by amide I/II protein backbone changes. Comparisons with redox IR spectra of small model ferredoxins demonstrate that these amide I/II changes arise primarily from characteristic structural changes local to the iron−sulfur centers, rather than from global structural alterations as has been suggested previously. Bands arising from the substrate ubiquinone were evident, as was a characteristic 1405 cm^{-1} band of the reduced form of the FMN cofactor. Other signals are likely to arise from perturbations or protonation changes of a carboxylic amino acid, histidine, and possibly several other specific amino acids. Redox difference spectra of center N2, together with substrate ubiquinone, were isolated from those of the other iron−sulfur centers by selective redox potentiometry. Its redox-linked amide I/II changes were typical of those in other 4Fe-4S iron sulfur proteins. Contrary to published data on bacterial complex I, no center N2 redox-linked protonation changes of carboxylic amino acids or tyrosine were evident, and other residues that could provide its redox-linked protonation site are discussed. Features of the substrate ubiquinone associated with the center N2 spectrum were particularly clear, with firm assignments possible for bands from both oxidized and reduced forms. This is the first report of IR properties of ubiquinone in complex I, and the data could be used to estimate a stoichiometry of 0.2−0.4 per complex I.

Complex I is the least understood of the major respiratory complexes. It functions as a proton-motive NADH:ubiquinone oxidoreductase in the respiratory chains of bacteria, plants, yeasts, and animals. Bacterial homologues are composed of 13−14 polypeptides (0.5 MDa) forming a minimal catalytic core that is present throughout the superfamily. Mammalian complex I has 32 additional subunits (*1*), which increase the molecular mass to approximately 1 MDa; the majority of them have no identifiable function. Single particle image reconstruction has revealed that complex I from all sources has an L-shaped structure, formed from a hydrophobic membrane arm and a hydrophilic arm (*2*−*4*), although a controversial 'horseshoe' shape has been reported more recently (*5,* 6). In bovine complex I, whose redox centers have been analyzed in greatest depth, the hydrophilic domain contains the NADH binding site, a noncovalently bound flavin mononucleotide (FMN; $E_{m7} = -340$ mV (*7, 8*)) and six EPR-detectable iron−sulfur (Fe−S) centers. A recent topology map of the Fe−S centers in complex I from *Thermus thermophilus* (*9*) supports their function as an electron-transfer pathway. However, one of the centers, 2Fe-2S center N1a, is placed on a limb separate from the main pathway. In addition the midpoint potential of this center ($E_{m7} = -380$ mV (*8, 10*)) is lower than the other components. Hence, its functional significance remains unclear, and it may have a role unrelated to the main electron-transfer pathway (*9*). The 2Fe-2S center N1b and the 4Fe-4S centers N3, N4 and N5 are roughly isopotential with E_{m7} values in the range −240 to −270 mV (*8, 10*), and two further 4Fe-4S centers, N6a and N6b, which have not been observed by EPR, are also present (*11*, *12*). The topology map (*9*) clearly indicates that these form an extended electron-conducting wire of sequence N3−N1b−N4−N5−N6a/b−N6b/a that conducts electrons across a distance of around 84 Å from FMN to the highest potential Fe−S center, the 4Fe-4S center N2 ($E_{m7} = +50$ to −150 mV (*8, 10, 13, 14*)). The core subunits of the hydrophobic arm are predicted to contain in excess of 50 transmembrane α-helices (*15*) but have no well-

† This work was supported by a UK BBSRC Studentship to D.M., grants of the Deutsche Forschungsgemeinschaft SFB472/P2 to U.B. and V.Z., and the Medical Research Council and the European Union Mitocombat Program to J.H. and R.S.

* Corresponding author. Tel. (+44)-(0)20 76797746; Fax. (+44)-(0)20 7679 7096; E-mail: prr@ucl.ac.uk.

‡ University College London.

§ Universität Frankfurt.

|| Medical Research Council Dunn Human Nutrition Unit.

[1] Abbreviations: FMN, flavin mononucleotide; Fe−S, iron−sulfur; FTIR, Fourier transform infrared; ATR, attenuated total reflection; *Y. lipolytica*, *Yarrowia lipolytica*; ISPs, iron sulfur proteins; E_{m7}, midpoint potential at pH 7 versus the standard hydrogen electrode.

10.1021/bi052561e CCC: $33.50
Published on Web 04/08/2006

characterized redox cofactors. Preliminary UV and infrared evidence for a redox-active chromophore in this domain has been reported (*16*), but its existence and nature remain uncertain, as do the number and location(s) of the ubiquinone binding site(s) (*17*).

Center N2 is of special interest as its midpoint potential has a redox-linked protonation site (*10*) that may be relevant to the protonmotive mechanism (*8, 18*). Furthermore, EPR data have provided strong indications that it can interact magnetically with ubisemiquinone (*19, 20*) and so is likely to be the immediate electron donor to substrate ubiquinone. Homology modeling with NiFe hydrogenases (*21*−*23*) and mutagenesis work (*24*) suggest that center N2 resides at the interface between the 49 kDa and PSST subunits (*14, 25*).

The Fe−S centers and ubiquinone have poor visible/UV signatures, and to date, the majority of mechanistic information on electron-transfer cofactors has come from EPR spectroscopy detection of reduced forms of Fe−S centers and semiquinone forms of ubiquinone and FMN (*8*). Fourier transform infrared (FTIR) spectroscopy has been used extensively to probe structural changes in individual cofactors and amino acids in proteins and offers a complementary method for the study of complex I (*26, 27*). Several reports of application of transmission FTIR to *Escherichia coli* complex I and its NADH dehydrogenase subfragment have appeared (*16, 28*−*30*) in which IR redox difference spectra have been interpreted in terms of large conformational changes of polypeptide (*30*), redox changes of FMN (*28*), and specific redox-linked protonation changes of carboxylic acids (*28*) and tyrosine (*29*). Attenuated total reflection (ATR)-FTIR spectroscopy (*31*−*33*) provides a flexible alternative to transmission FTIR, and it increases the range of protein manipulations that may be studied (*34*). Here we report the application of ATR-FTIR electrochemical difference spectroscopy to provide the first IR data on eukaryotic mitochondrial complex I isolated from the obligate aerobic yeast *Yarrowia lipolytica* (*35*) and from bovine heart. The aim was to further investigate the nature of redox-linked conformational and amino acid signals and to extend band assignments to cofactors and ubiquinone. The study advances previous IR work on bacterial complex I with radically different interpretations of amide I/II and amino acid signals, with separation of center N2 and ubiquinone signals by selective reduction and with detection for the first time of characteristic bands from substrate ubiquinone and the reduced flavin cofactor.

MATERIALS AND METHODS

Proteins. Y. lipolytica complex I was prepared as described in (*24*) and bovine complex I as described in ref *36*. In both cases, small aliquots were stored at −80 °C until required. The 2Fe-2S ferredoxin from parsley chloroplasts was purified as described in (*37*). 4Fe-4S ferredoxins from *Desulfovibrio africanus* and *Clostridium* sporogenes were supplied by Prof. Dick Cammack, Kings College London.

Sample Preparation for ATR-FTIR Spectroscopy. Approximately 0.1 mg complex I was diluted into 2 mL of 20 mM potassium phosphate, 0.0075% (w/v) sodium cholate, and 0.0075% (w/v) octylglucoside at pH 8.0 and pelleted by centrifugation at 390 000 g_{av} for 30 min. The resulting pellet was resuspended and centrifuged at 300 000 g_{av} for 20 min, and this was repeated with 1 mM potassium phosphate at pH 8.0. The final pellet was resuspended in 10 μL of distilled water and divided into 2 μL aliquots which were either diluted to 6 μL and applied directly to the ATR-FTIR silicon microprism (SensIR; 3 reflection; 3 mm surface diameter) or stored at −80 °C for later use. The 6 μL aliquot was dried onto the microprism under a gentle stream of air prior to rehydration with 10 μL of 20 mM potassium phosphate, 200 mM potassium chloride at pH 6.0 or 8.0. Drying and rehydration were monitored from absolute ATR-FTIR absorption spectra measured at different stages during preparation of a rehydrated protein film (Figure 1). The spectrum of the initial suspension of protein was dominated by the O−H scissoring mode of water at 1638 cm^{-1} (trace A). After drying, the spectrum was dominated by amide I (peak at 1650 cm^{-1}) and amide II (peak at 1538 cm^{-1}) protein bands (trace B), together with structural water that remained bound within the protein regardless of drying time. A band at 1740 cm^{-1} can also clearly be seen that is due primarily to the lipid ester bond (*38*) and can provide a useful means of estimating lipid/protein ratio. Subsequent rehydration caused a decrease in the amplitude of the protein and lipid bands as the film expanded, together with an increased water contribution beneath the amide I envelope (trace C). In general, the sample became sufficiently stable for data acquisition within 30 min of rewetting. A stable amide II signal after rehydration of $\Delta A \geq 0.1$ was acceptable for acquisition of difference spectra of adequate signal/noise.

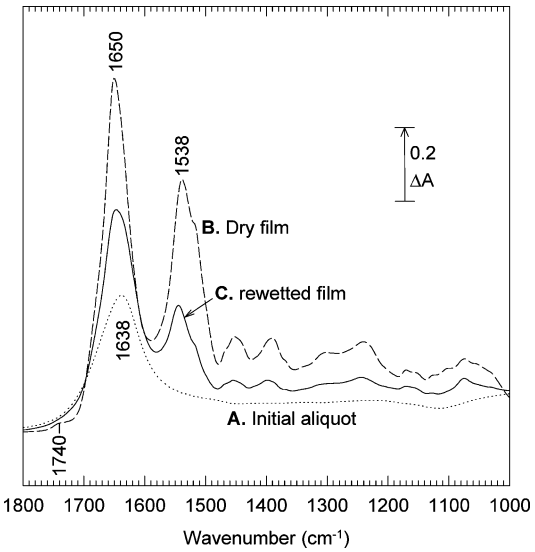

FIGURE 1: ATR−FTIR absorption spectra of a sample of *Y. lipolytica* complex I during rehydrated film preparation. A 6 μL aliquot of detergent-depleted protein suspended in H_2O (see Materials and Methods) was placed on the silicon microprism, and the absorption spectrum was recorded (trace A). The absorption spectrum was recorded again after the sample had been dried under a gentle stream of dry air (trace B). Finally, the sample was rehydrated and the absorption spectrum recorded again (trace C).

H/D Exchange. For deuterium oxide (D_2O) exchange, sample preparation and ATR measurements were performed throughout by substitution of D_2O buffers at appropriate pD (assuming pD is equal to the pH meter reading + 0.4 (*39*)). Preincubation of samples in D_2O overnight at 4 °C before dilution and washing as described above increased the amount of H/D exchange, the final extent of which was estimated to be >90% using published methods (*40*).

Redox Cycling and Data Acquisition. All potentials are quoted versus the standard hydrogen electrode. Automated cycling between reduced and oxidized states was achieved with an in-house constructed electrochemical cell operating in conventional three electrode mode (*34*, *41*). The potential between working and reference electrodes was set with a Model 704 PAR potentiostat and modulated with a computer-controlled offset device. The working electrode was a 9 mm glassy carbon disk, cleaned before use with a paste of 0.03 mm alumina powder, which formed the top of a sample chamber of less than 0.3 mm thickness. The auxiliary electrode was a platinum sheet (40 mm^2 surface area) connected to the sample by a porous glass frit, and a Ag/AgCl reference electrode provided the reference voltage (+204 mV). Redox mediation between glassy carbon and protein film was provided by a buffer of 20 mM potassium phosphate, 200 mM potassium chloride, 0.1 mM methyl viologen ($E_{m7} = -446$ mV), and 1 mM potassium ferricyanide ($E_{m7} = +420$ mV) at pH 6.0 or 8.0. For full redox difference spectra, the applied potential was routinely alternated between −425 and + 425 mV. For selective reduction of center N2, 0.1 mM anthraquinone-2,6-disulfonate ($E_{m7} = -185$ mV) was also included and the applied potential was cycled between −425, −220, and + 425 mV.

ATR-FTIR spectra were recorded with a Bruker ISF 66/S spectrometer, fitted with a liquid nitrogen-cooled MCT-A or -B-type detector. All frequencies quoted are accurate to ±1 cm^{-1}. Typically, difference spectra (presented as reduced *minus* oxidized differences) consisted of data averaged from 50 oxidative and 50 reductive cycles, with individual spectra averaged from 1000 interferograms at 4 cm^{-1} resolution. Where necessary, baseline corrections due to protein swelling/shrinkage and contributions from mediators and buffer were removed by interactive subtraction (see Figure 2).

RESULTS

The figures described below contain a large number of components and not all are discussed here. For clarity, only bands that were consistently found above the signal/noise, and for which firm or tentative assignments are made below, have their frequencies labeled.

Y. lipolytica Complex I Redox Difference Spectra. Effects of pH, H/D Exchange, and Global ^{15}N Labeling. Averaged ATR-FTIR redox difference spectra of *Y. lipolytica* complex I at pH 6.0 are shown in Figure 2 in both reductive (trace A) and oxidative (trace B) directions. These spectra are nearly mirror images of each other, confirming the reversibility of the transitions. The final reduced *minus* oxidized difference spectrum (trace E) was generated by averaging these reductive and oxidative data (trace C) followed by interactive subtraction of changes due to protein swelling/shrinkage, redox mediators, and buffer. In practice, these adjustments were small; trace D is typical and shows the sum of all adjustments from protein swelling/shrinkage, mediators and buffers that were subtracted from trace C to produce trace E. An equivalent reduced *minus* oxidized difference spectrum at pH 8.0 (trace F) was obtained in the same manner and is very similar to that at pH 6.0. Equivalent reduced *minus* oxidized difference spectra recorded in D_2O media at pD 6.0 and 8.0 after H/D exchange (see Methods) are shown in Figure 3A and in material which had been globally ^{15}N-labeled in Figure 3B. In both cases, for comparison purposes the spectra are overlaid on the spectra in H_2O media from Figure 2 after normalization so that the amide I amplitudes were roughly comparable. The differences between these spectra were used to confirm assignments of bands to amide I/II conformational changes, FMN, and bound ubiquinone, as well as suggesting contributions to spectra from several specific types of amino acids, as described below.

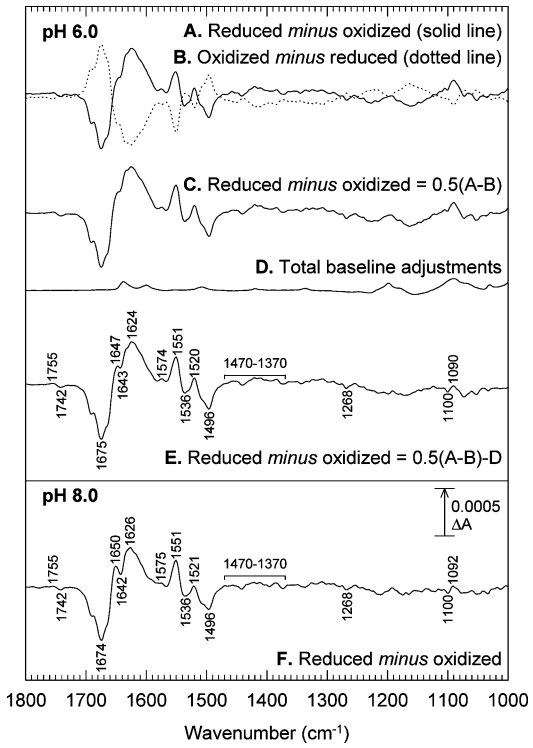

FIGURE 2: Reduced *minus* oxidized difference spectra of *Y. lipolytica* complex I at pH 6.0 and pH 8.0. Averaged data from 70 reduced *minus* oxidized or 70 oxidized *minus* reduced cycles at pH 6.0 are shown in traces A and B, respectively. The final reduced *minus* oxidized spectrum (trace E) was produced by averaging traces A and B and subtracting contributions from buffer/mediator/protein film expansion (shown combined in trace D). An equivalent reduced *minus* oxidized spectrum at pH 8.0 is shown in trace F.

Redox Separation of Center N2 at pH 8.0. The redox potential of center N2 of *Y. lipolytica* complex I has been reported to be −140 mV at pH 7 (*14*). Hence, reduced *minus* oxidized difference spectra of *Y. lipolytica* complex I were obtained using −220 mV and +425 mV as reducing and oxidizing potentials, respectively (see Figure 4, trace A) in order to selectively reduce center N2. Stepwise reduction between −130 and −220 mV confirmed that the species undergoing oxidation/reduction had a midpoint potential close to the expected value and that the potential of −220 mV caused essentially complete reduction with no evidence of change of shape that would indicate that the lower potential Fe−S centers were starting to become reduced. A reduced *minus* oxidized difference spectrum between −425 and −220 mV was also recorded in the same sample in order to reduce the lower potential 'non-N2' components (trace B). This was summed with trace A to produce trace C. The similarity of trace C to the equivalent full reduced *minus* oxidized spectrum from Figure 2 (reproduced as trace D in Figure 4) indicates that the full complement of detectable redox centers were being titrated.

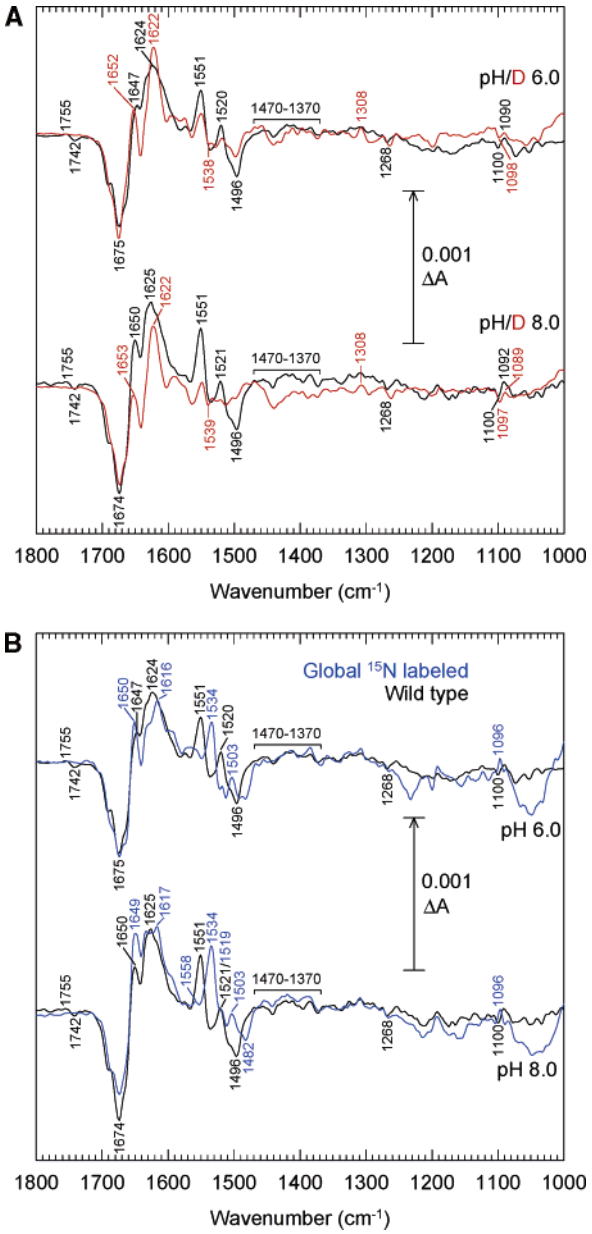

FIGURE 3: Effects of H/D exchange and global ^{15}N labeling on redox difference spectra of *Y. lipolytica* complex I at pH 6.0 and 8.0. A. Reduced *minus* oxidized spectra at pH 6.0 and 8.0 are shown with equivalent spectra recorded in D_2O media, after completion of H/D exchange, overlaid. B. Reduced *minus* oxidized spectra at pH 6.0 and 8.0 are shown with equivalent spectra for global ^{15}N-labeled complex I overlaid.

The −220 *minus* +425 mV difference spectrum, which arises from center N2 and bound ubiquinone, is shown in more detail in trace E, and an equivalent redox difference spectrum in D_2O media has been overlaid for comparison (trace F). Effects of global-^{15}N-labeling on this spectrum in D_2O were compared by overlaying equivalent spectra in D_2O of ^{15}N (trace G) and ^{14}N (trace F) labeled proteins. These data can be interpreted as arising from a conformational change around center N2 that is typical of a 4Fe-4S Fe−S, together with signals arising from bound ubiquinone in its substrate binding site (see Discussion).

Comparison of Y. lipolytica and Bovine Complex I Redox Difference Spectra at pH 6.0. A reduced *minus* oxidized difference spectrum of bovine complex I was recorded under conditions equivalent to those used to obtain the redox

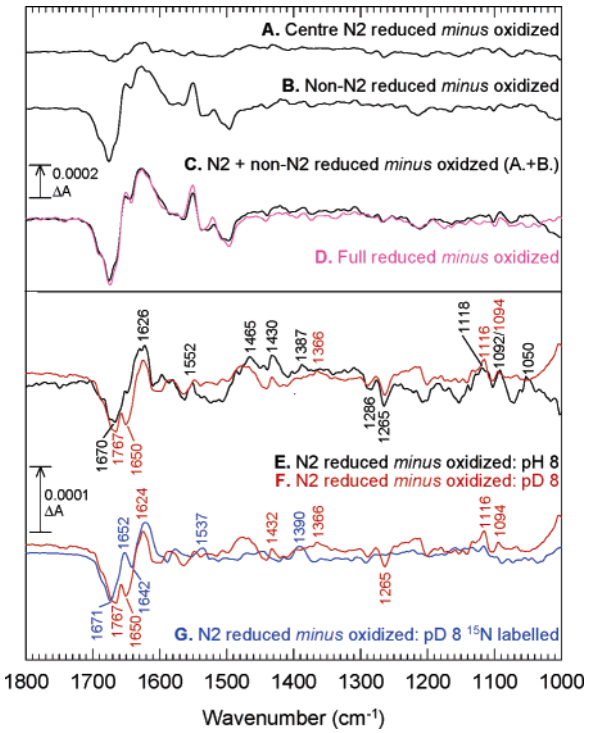

FIGURE 4: Redox difference spectra demonstrating the resolution of center N2 in *Y. lipolytica* complex I by selective redox poising at pH 8.0. Electrochemical conditions of −220 mV (reducing) and + 425 mV (oxidizing) were used to selectively reduce/oxidize iron−sulfur center N2 (E_{m7} = −140 mV) (trace A). As a control, difference spectra were recorded for transitions between −425 mV and −220 mV i.e., reduction/oxidation of all components except center N2 (trace B); the sum of traces A and B (trace C) is comparable to a full reduced *minus* oxidized spectrum at pH 8 (trace D, a reproduction of trace F of Figure 2). Effects of H/D exchange are illustrated by a center N2 spectrum in D_2O (red trace F) overlaid on that in H_2O (trace E). Effects of global ^{15}N labeling combined with H/D exchange is illustrated by a center N2 spectrum in D_2O of ^{15}N-labeled material (blue trace G) overlaid on the ^{14}N control sample in D_2O (trace F).

difference spectrum of *Y. lipolytica* complex I at pH 6.0. For comparison, this spectrum is shown in Figure 5 together with the equivalent from *Y. lipolytica* complex I (trace E of Figure 2). The overall shapes of the spectra in the amide I/II regions are similar. However, there are differences in some of the more detailed features that in large part arise because of a low ubiquinone content in the bovine samples, resulting in very small IR contributions from ubiquinol/ubiquinone and hence clearer definition of the 1405 cm^{-1} N5−H in-plane bending mode (*42*) of reduced FMN (see Discussion).

DISCUSSION

Peptide Backbone Changes and Protein Stability. The reduced *minus* oxidized difference spectra of complex I are dominated by large changes in the 1700−1590 cm^{-1} and 1570−1490 cm^{-1} regions. These changes are very similar to those found with *E. coli* complex I (*28*) where they were assigned to amide I/II changes that might be associated with large conformational changes of functional significance in relation to protonmotive mechanism (*30*). The effects of H/D exchange and global ^{15}N-substitution reported here confirm that they are indeed predominantly amide I/II changes.

To investigate their significance further we recorded reduced *minus* oxidized difference spectra of several small

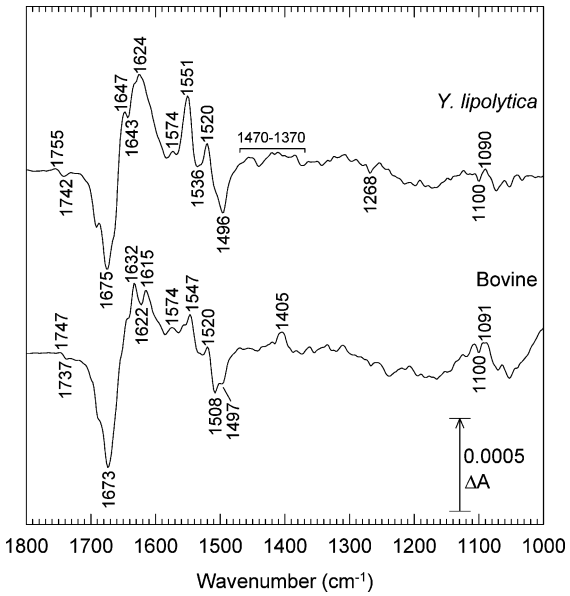

FIGURE 5: Electrochemically induced reduced *minus* oxidized difference spectra of bovine and *Y.* lipolytica complex I at pH 6.0. The presented spectra for bovine and *Y. lipolytica* complex I were acquired using the same experimental conditions (see text).

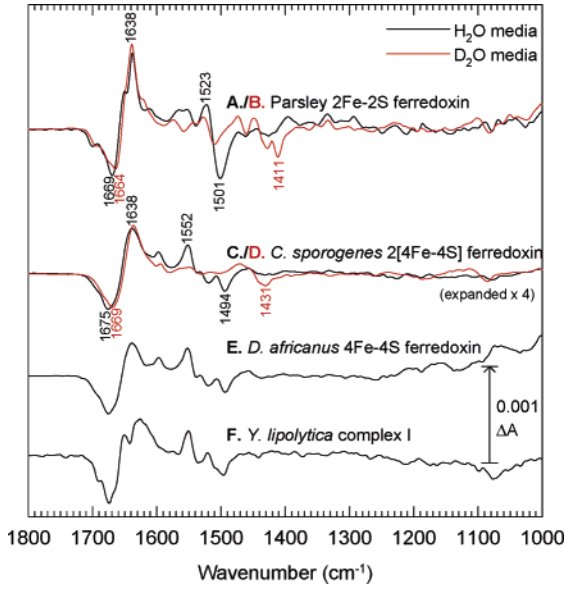

FIGURE 6: Redox difference spectra of model ISPs in comparison to complex I. The soluble ISPs were exchanged into 0.1 M potassium phosphate and 100 mM KCl at pH 8.0 by repeated dilution and concentration using a centrifugal concentrator. 50 μM methyl viologen was added as a redox mediator and the sample was placed in the electrochemical ATR-FTIR cell. Potential was switched between −500 and + 200 mV, allowing 8 min for redox equilibration. For H/D exchange, samples were washed and concentrated in equivalent D_2O media. Reduced *minus* oxidized and oxidized *minus* reduced spectra (each the average of 1000 interferograms at 4 cm^{-1} resolution) were averaged to produce the spectra shown. Spectra are: 2 mM parsley 2Fe-2S ferredoxin in H_2O (trace A, average of 106 spectra) or D_2O (trace B, average of 54 spectra); 2.5 mM *C. sporogenes* 4Fe-4S ferredoxin in H_2O (trace C, average of 98 spectra) or D_2O (trace D, average of 70 spectra); 0.42 mM *D.* africanus 4Fe-4S ferredoxin in H_2O (trace E, average of 258 spectra); *Y. lipolytica* complex I film in H_2O media (trace F), data from Figure 2, reproduced for comparison.

2Fe-2S and 4Fe-4S iron sulfur proteins (ISPs) and compared them to a typical spectrum of complex I (Figure 6). A more extensive survey of IR redox spectra of small ISPs (Marshall, Cammack, Hatchikian and Rich, unpublished) has indicated that the amide I/II signatures of the 2Fe-2S and 4Fe-4S ISPs are, as shown, characteristically different from each other, but tend to be the same within each distinct ISP subclass. This presumably reflects the fact that the redox-induced changes within the protein folds around the Fe−S centers are conserved within ISP types. In some instances, structural data are available for both oxidized and reduced forms (for example, for *D. africanus* 4Fe-4S ferredoxin (*43*, *44*)) and the nature of the redox-sensitive local conformational change can be visualized (*45*).

The overall shape of the amide I/II region of complex I is remarkably similar to the pattern seen in the small model ISPs both in H_2O and in D_2O, being most similar to that of the 4Fe-4S type, consistent with its complement of 6 4Fe-4S centers and two 2Fe-2S centers. In fact, the magnitudes of the amide I/II changes in the complex I film (which we estimate to contain around 0.25−0.5 mM complex I, thus 1.5−3 mM 4Fe-4S and 0.5−1 mM 2Fe-2S prosthetic groups) were roughly equivalent to the magnitudes obtained from a 2 mM soluble protein. Hence, it is clear that the amide I/II changes in complex I arise primarily from redox-linked changes of local protein folds around the Fe−S centers that tend to be preserved in the ISP subclasses generally. This conclusion contrasts with the interpretation of similar changes in the redox IR difference spectra of *E. coli* complex I (*30*) where it was suggested that they might indicate more global conformational effects related to the coupling mechanism. However, although the IR data do not support such changes, it should be noted that the IR data do not address whether large domain movements involving only a few residues in the hinge region, or conformational changes in short-lived intermediates, might instead occur.

The complex I preparations used here require additional lipid in order to observe maximal NADH-decyl-ubiquinone oxidoreductase activity (*46*); most probably, lipid is required for rapid exchange of substrate ubiquinone with its binding site. However, the complexes are still likely to be in their native states and display rapid NADH-hexaammineruthenium oxidoreductase activities (*47*) even without lipid supplementation. This activity remained in samples that had undergone a drying/rehydration cycle, and furthermore the redox centers in the protein film could be reduced by NADH (unpublished data). Hence, it may be concluded that the complex I samples are in a native state, although it would be of interest in future to extend the studies to preparations in which their NADH-decyl-ubiquinone oxidoreductase activities have been reactivated (*36*, *48*). No large differences in redox difference spectra, apart from some variation in the magnitude of a presumed carboxylic acid change around 1740 cm^{-1} (see below), nor differences in long-term stability of samples during data acquisition, were evident in samples at either pH 6.0 and 8.0, indicating that these eukaryotic enzymes are stable over a larger pH range than complex I from *E. coli* (*30*). This additional stability is probably provided by the numerous supernumerary subunits that are associated with the eukaryotic enzymes (*11*, *49*) and which bind around the core subunits (*15*) and might also be enhanced by the protein−protein interactions within the tightly packed layer.

Changes Associated with Ubiquinone. Fe−S modes are not expected to contribute at frequencies above 800 cm^{-1}, and therefore all changes should arise from protein, FMN,

ubiquinone, and possibly as-yet unrecognized redox groups. The redox IR spectra of model ubiquinone (*50*−*55*) have been described in detail in both H_2O and D_2O media. Such model spectra provide valuable templates for recognition of ubiquinone (and FMN, see below) bands in the complex I spectra.

Biochemical analyses of the complex I preparations have shown that substoichiometric ubiquinone typically remains bound to the *Y. lipolytica* complex I preparations (*46*). Particularly useful IR markers for ubiquinone are H/D-insensitive troughs at 1288 and 1262 cm^{-1} that involve the methoxy groups and a sharp C═C band at 1610 cm^{-1} (*50*−*54*), and for ubiquinol are four bands between 1492 and 1387 cm^{-1} and five between 1112 and 963 cm^{-1} that show a characteristic pattern of H/D-sensitivity (*55*). Some indications of the strongest of the methoxy-related bands of ubiquinone are evident in the full redox spectra of *Y. lipolytica* complex I as a 1268 cm^{-1} trough (Figure 2). Ubiquinone-related bands of *Y. lipolytica* should become much more evident in the reduced *minus* oxidized spectra of center N2 alone (Figure 4), since the ubiquinone would be expected to also undergo redox changes in this potential range, and this is indeed the case: H/D insensitive troughs at 1286 and 1265 cm^{-1} can be assigned to loss of bound ubiquinone. H/D-insensitive peaks at 1465 and 1430, a peak at 1387 cm^{-1} which is downshifted to 1366 cm^{-1} with H/D exchange, and 1092 and 1050 cm^{-1} peaks that are lost in D_2O with appearance of a more prominent peak at 1116 cm^{-1} can all be assigned to ubiquinol formation. The amount of redox-active ubiquinone, estimated by comparison of the size of the 1265 cm^{-1} methoxy trough with the size of the same band in solutions of free ubiquinone (not shown), was estimated to be 0.2−0.4 ubiquinone per complex I, consistent with biochemical estimates (*46*) and demonstrating that the IR method can provide a convenient means of quantitation of ubiquinone in such materials. The slight shifts in positions of the features of complex I-bound ubiquinone in relation to those of free ubiquinone (*55*) indicate that it is bound in a specific site rather than being nonspecifically associated (*56*). Its substoichiometry strongly suggests that it is the substrate Q-site that is partially occupied rather than indicating a very tightly bound form, the possibility of which is ruled out by these data. The level of occupancy by ubiquinone appears to be somewhat variable in different preparations. For example, the redox difference spectrum of the bovine complex I sample (Figure 5) shows a much weaker ubiquinone signature, indicating a lower retained ubiquinone content in this preparation. In addition, the signature ubiquinone redox bands are virtually absent from the ^{15}N-labeled *Y. lipolytica* complex I sample due to a particularly low retained level of ubiquinone in this sample. Such variable levels of ubiquinone in substrate Q-sites (and of retained lipid) is not uncommon in purified preparations of many membrane-derived Q-reactive redox enzymes.

Changes Associated with FMN. The redox IR spectra of FMN (*28*, *42*) have been described in detail in both H_2O and D_2O media. Some further details of FMN redox IR spectra at pH/pD 6.0 and 8.0 are shown in Figure 7 and are consistent with published spectra where some assignments of principle bands have been made (*28*). The most prominent features are a large trough at ∼1547 cm^{-1} (assigned to a ν(C═C) mode of FMN (*28*)) and H/D exchange-sensitive

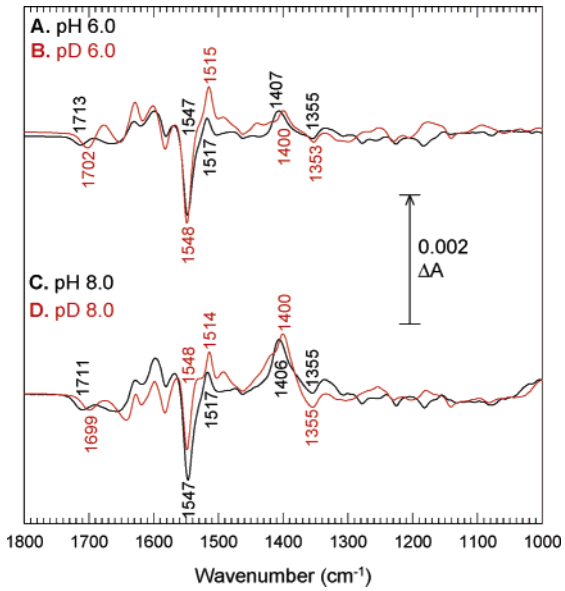

FIGURE 7: Redox difference spectra of FMN at pH 6.0 and 8.0. Reduced *minus* oxidized difference spectra of a solution of 2 mM FMN (E_{m7} = −219 mV) in 20 mM potassium phosphate and 200 mM potassium chloride at pH/D 6.0 and 8.0. Reducing conditions were −550 mV and oxidizing conditions were +200 mV and equilibration occurred after 6 min.

peaks at ∼1517 (assigned to hydrogen in-plane bending) and ∼1406 cm^{-1} (assigned in part to N5−H in-plane bending (*42*)). The 1406 cm^{-1} band is increased in intensity relative to other bands at pH 8.0, indicating that it is most prominent in the anionic $FMNH^-$ form (pK_a of $FMNH_2/FMNH^-$ = 6.7 in aqueous media (*57*) and 7.1 in bovine complex 1 (*7*)). *Y. lipolytica* complex I spectra in H_2O media (Figure 2) exhibit several overlapping bands in the 1470−1370 cm^{-1} region that arise in large part from ubiquinol (see above). The model FMN data (Figure 7) predict peaks at 1406 cm^{-1} for reduced protein-bound FMN with intensities in the range of (0.5−5) × 10^{-4} and (1−2) × 10^{-4} ΔA at pH 6.0 and 8.0, respectively, and this will sit between the 1430 and 1387 cm^{-1} peaks of ubiquinol (*55*), giving rise to the rather flat, broad overlapping peaks in this region in the spectra of Figures 2 and 3. In contrast, a distinct 1405 cm^{-1} peak of reduced FMN is evident in the bovine spectrum (Figure 5) of roughly the expected intensity, presumably in its $FMNH_2$ form at pH 6.0.

The largest band of free FMN, the ν(C═C) 1547 cm^{-1} trough, whose ΔA from the model spectra is expected to be (2−3) × 10^{-4}, is obscured by the very large amide II changes of the Fe−S centers. After H/D exchange, which shifts the majority of the amide II changes away from this region, the full reduced *minus* oxidized *Y. lipolytica* spectra do have a small trough at 1538 cm^{-1} (see Figure 3A) that likely arises from this H/D exchange-insensitive ν(C═C) mode of the bound FMN. Hellwig et al. (*28*) have previously assigned a band at 1548 cm^{-1} in redox difference spectra of the NADH dehydrogenase fragment of *E. coli* complex I primarily to FMN. Comparison with the redox spectra of model ISPs (Figure 6), however, strongly suggests that this arises predominately from the flanking amide II changes of polypeptide around the Fe−S centers. In this same work, an indistinct shoulder at 1710 cm^{-1} was also suggested to arise at least in part from an equivalent of the 1713 cm^{-1} carbonyl band of free FMN, although it was noted that a lack of H/D

sensitivity made this assignment questionable, and a band close to 1400 cm^{-1} was assigned to an amino acid carboxylate group rather than to reduced FMN (*28*). In the spectra reported here, there is no clear 1710 cm^{-1} band that could reasonably be attributed to this FMN carbonyl group, which in any case is expected to be of low intensity and likely to be obscured by the strong amide I changes associated with redox changes of the Fe−S centers in our spectra. Hence, in summary, the 1406 cm^{-1} band of reduced FMN seems to be the best IR marker band, at least for eukaryotic complex I, even though in full redox spectra it can be obscured by overlapping ubiquinol bands.

IR Characteristics of Center N2. The ability to selectively reduce center N2 and bound ubiquinone at the reducing potential used here of −220 mV is consistent with their higher midpoint potentials relative to the other Fe−S and FMN cofactors. The center N2 redox IR spectra are dominated by amide I/II changes, and these again closely resemble those seen in small soluble 4Fe-4S proteins (Figure 6), indicating that center N2 retains characteristics of the 4Fe-4S class despite the fact that it may be ligated between two proteins (*14*, *25*). Furthermore, because only a single Fe−S is reduced, the bands arising from the substoichiometric bound ubiquinone and ubiquinol that are more weakly evident in the full redox spectra are now much more prominent, as discussed above.

Of particular interest in relation to possible coupling mechanism is the nature of the protonation site that is redox-linked to center N2 (*12*). In previous work on *E. coli* complex I, it was reported that reduction of center N2 at pH 6.0 was associated with deprotonation of a carboxylic amino acid (*28*) together with protonation of two tyrosine groups (*29*). These tyrosines were suggested by site-directed mutagenesis to be Y114 and Y139 on the NuoB (PSST) subunit. Clearly, such unusual protonation chemistry might be expected to play a major role in the proton/electron coupling mechanism of complex I. However, the 1755/1742 cm^{-1} carboxylic acid feature seen in the full redox spectra of eukaryotic complex I (Figures 2 and 5) appears to be associated only with the lower potential 'non-N2' components in experiments such as those in Figure 4, and the redox spectra of center N2 show no clear evidence for equivalent redox-linked protonation changes of either tyrosines or carboxylic acids in the eukaryotic protein. This is particularly clear in center N2 redox spectra in D_2O and after ^{15}N-labeling (traces F and G, Figure 4): although there is a peak at 1552 cm^{-1} that could conceivably arise from carboxylate formation on reduction, its sensitivity to H/D exchange and to ^{15}N-labeling rules this out and strongly suggests that it is instead an amide II feature. Similarly, there are no ^{15}N-insensitive bands in the 1500 cm^{-1} region that would indicate tyrosine changes. As a result, it is concluded that protonation changes of carboxylic acids or tyrosine are not linked to center N2 redox changes in eukaryotic complex I. Nevertheless, equivalents of tyrosines Y114 and Y139 are conserved in both the *Y. lipolytica* and bovine PSST subunits so some consideration of the possible origin of the very different behaviors is desirable. In the case of *E. coli* center N2, its midpoint potential is reported to be −210 mV at pH 7, a value very close to the isopotential group of N1b, N3, N4, and N5 (E_{m7} −280 to −240 mV). As a result, the data on center N2 in (*28*) could not be obtained by selective reduction, and instead it was necessary to subtract the IR redox difference spectrum of a fragment (thought to contain all redox groups except center N2) from the IR redox spectrum of the intact complex. In contrast, center N2 in *Y. lipolytica* complex I, like the bovine enzyme (*8*), has a midpoint potential ($E_{m7} = -140$ mV (*14*)) that is high enough above the other Fe−S centers (E_{m7} −250 mV or below (*8*)) that it could be resolved directly in the intact complex by selective reduction without a need to compare different protein preparations. Given the very different redox midpoint potentials of the *E. coli* and eukaryotic centers N2, it is conceivable that their redox-linked chemistry is also very different. However, it is also feasible that the *E. coli* complex I fragment that has lost center N2 has major alterations to other parts of the protein structure that behave differently in the fragment compared to the intact enzyme and this could give rise to the additional signals that appear to be associated with center N2 in the *E.* coli complex I.

Hence, the nature of the redox-linked protonation site of center N2 remains unclear, though the present work argues strongly against the involvement of a network of tyrosines/carboxylic acid changes (*28*, *29*). The H/D-exchange and ^{15}N-substitution effects on the amide I envelope raise the possibility that a lysine or arginine could provide the site. In addition, the bandshifts in the 1100 cm^{-1} region in Figure 4 may not be fully accounted by the hydroxyl-related bands of ubiquinol in this region (for example, a positive band at 1116 cm^{-1} is present in the ^{15}N-substituted sample of trace G, Figure 4 even although the ubiquinone content is very low), and this raises the alternative possibility that the redox reaction of center N2 might be associated with histidine protonation changes. This would be consistent with other data that have implicated histidine as the redox-linked protonation group (*58*). Such possibilities can be tested with further isotope replacements and mutagenesis.

Amino Acid Side Chains. Besides the protonation site that is redox-linked to center N2, additional band changes arising from environmental, redox, or protonation state changes of specific types of amino acid residues might also be reasonably expected to contribute to the full redox difference spectra. Some possible assignments may be suggested by comparisons with IR databases of amino acid vibrational spectra ((*34*, *59*−*61*) and references therein). The principle bands of several amino acids tend to occur at frequencies within the amide I/II envelopes, and this makes their detection difficult. For example, lysine, arginine, glutamine, and asparagine all have very strong vibrations in the 1690−1620 cm^{-1} range. In contrast to amide I bands which are very weakly downshifted in D_2O or by ^{15}N-substitution (*62*), bands of these amino acids in this region are very strongly shifted both with H/D exchange (*60*) and with ^{15}N-substitution (*63*). Figures 3A and 3B show that H/D and $^{14}N/^{15}N$ exchanges do cause significant changes in the central part of the amide I region that are larger than might arise from amide I bands alone. Hence, significant redox-linked alterations of one or more of these amino acid types might be occurring that are worthy of further specific investigations.

Easier to assign are bands of amino acids that occur in less congested regions of the spectra. One such signal that is consistently evident in the full reduced *minus* oxidized spectra (Figures 2, 3, and 5) is a peak/trough close to 1090/1100 cm^{-1}. Protein bands in this region result from changes in environment or protonation state of histidine (*64*−*66*). The

trough is only slightly downshifted in D_2O but changes dramatically with ^{15}N-labeling to give predominantly a 1096 cm^{-1} peak. This behavior is consistent with the protonation to the imidazolium form of a neutral histidine that is protonated in the N_π position (*64*, *66*).

A second signal that is consistently evident is a trough/peak at 1742/1755 cm^{-1} (1737/1747 cm^{-1} in bovine). These frequencies are characteristic of a protonated aspartic or glutamic acid residue whose environment is perturbed by one or more redox centers (*60*). However, although consistently present, its size relative to other bands has proved to be variable within a factor of 2−3, with its size in Figure 2 data being at the higher end of the range. In addition, although H/D exchange causes its loss, possibly due to the expected downshift where it might become obscured by the amide I envelope edge, it also appears to be lost in the ^{15}N-substituted samples, a substitution that should not affect carboxylic acid vibrations. Hence, further investigations are required to determine whether this band arises from a carboxylic acid, from the ester bond of a bound lipid (*38*) or from an as-yet unknown functional moiety.

A significant body of data is available on tyrosine, tyrosinate, and the related *p*-cresol in H_2O and D_2O (*60*), and on specific isotope effects both for model compounds (*67*, *68*) and tyrosine in proteins (*29*, *68*, *69*). The most prominent band of tyrosine is its ν(CC) ring mode at 1515 cm^{-1}, shifting to 1495 cm^{-1} in the tyrosinate form. The complex I spectra are dominated by the very strong Fe−S amide II peak at 1520 cm^{-1} and this obscures tyrosine bands. However, this amide II band is strongly downshifted both by H/D exchange and by ^{15}N-labeling, whereas the tyrosine bands are little affected. Hence, the small bands remaining in the 1500 cm^{-1} region after these exchanges (Figures 3 and 4) could arise from redox-linked tyrosine changes.

In summary, we report here definitive assignments of IR signals to local conformational changes around the Fe−S centers and to FMN cofactor and ubiquinone substrate. In addition, we report a number of further bands that are consistently observed that should also arise from specific amino acid changes for which suggestions of possible assignments are made to guide further isotope replacement and mutagenesis investigations.

ACKNOWLEDGMENT

We are grateful to Santiago Garcia for expert technical assistance and Dr. Jacques Breton for useful discussions during the development of this method.

REFERENCES

1. Carroll, J., Fearnley, I. M., Shannon, R. J., Hirst, J., and Walker, J. E. (2003) Analysis of the Subunit Composition of Complex I from Bovine Heart Mitochondria, *Mol. Cell. Proteom. 2*, 117−126.
2. Friedrich, T. (1998) The NADH: ubiquinone oxidoreductase (complex I) from *Escherichia coli*, *Biochim. Biophys. Acta 1364*, 134−146.
3. Guenebaut, V., Schlitt, A., Weiss, H., Leonard, K., and Friedrich, T. (1998) Consistent structure between bacterial and mitochondrial NADH: Ubiquinone oxidoreductase (complex I), *J. Mol. Biol. 276*, 105−112.
4. Friedrich, T., and Böttcher, B. (2004) The gross structure of the respiratory complex I: a Lego System, *Biochim. Biophys. Acta 1608*, 1−9.
5. Böttcher, B., Scheide, D., Hesterberg, M., Nagel-Steger, L., and Friedrich, T. (2002) A novel, Enzymatically Active Conformation of the NADH: Ubiquinone Oxidoreductase (Complex I), *J. Biol. Chem. 277*, 17970−17977.
6. Sazanov, L. A., Carroll, J., Holt, P., Toime, L., and Fearnley, I. M. (2003) A role for native lipids in the stabilization and two-dimensional crystallization of the *Escherichia coli* NADH-ubiquinone oxidoreductase (complex I), *J. Biol. Chem. 278*, 19483−19491.
7. Sled, V. D., Rudnitzky, N. I., Hatefi, Y., and Ohnishi, T. (1994) Thermodynamic analysis of flavin in mitochondrial NADH: ubiquinone oxidoreductase (complex I), *Biochemistry 33*, 10069−10075.
8. Ohnishi, T. (1998) Iron−sulfur clusters/semiquinones in complex I, *Biochim. Biophys. Acta 1364*, 186−206.
9. Hinchliffe, P., and Sazanov, L. A. (2005) Organization of iron−sulfur clusters in respiratory complex I, *Science 309*, 771−774.
10. Ingledew, W. J., and Ohnishi, T. (1980) An analysis of some thermodynamic properties of iron-sulphur centres in site I of mitochondria, *Biochem. J. 186*, 111−117.
11. Hirst, J., Carroll, J., Fearnley, I. M., Shannon, R. J., and Walker, J. E. (2003) The nuclear encoded subunits of complex I from bovine heart mitochondria, *Biochim. Biophys. Acta 1604*, 135−150.
12. Hirst, J. (2005) Energy transduction by respiratory complex I − an evaluation of current knowledge, *Biochem. Soc. Trans. 33*, 525−529.
13. Wang, D.-C., Meinhardt, S. W., Sackmann, U., Weiss, H., and Ohnishi, T. (1991) The iron−sulfur clusters in the two related forms of mitochondrial NADH: ubiquinone oxidoreductase made by *Neurospora crassa*, *Eur. J. Biochem. 197*, 257−264.
14. Garofano, A., Zwicker, K., Kerscher, S., Okun, P., and Brandt, U. (2003) Two Aspartic Residues in the PSST-Homologous NUKM Subunit of Complex I from *Yarrowia lipolytica* Are Essential for Catalytic Activity, *J. Biol. Chem. 278*, 42435−42440.
15. Friedrich, T., Steinmüller, K., and Weiss, H. (1995) The proton-pumping respiratory complex I of bacteria and mitochondria and its homologue in chloroplasts, *FEBS Lett. 367*, 107−111.
16. Friedrich, T., Brors, B., Hellwig, P., Kintscher, L., Rasmussen, T., Scheide, D., Schulte, U., Mäntele, W., and Weiss, H. (2000) Characterization of two novel redox groups in the respiratory NADH: ubiquinone oxidoreductase (complex I), *Biochim. Biophys. Acta 1459*, 305−309.
17. Rich, P. R. (2003) The molecular machinery of Keilin's respiratory chain, *Biochem. Soc. Trans. 31*, 1095−1105.
18. Brandt, U. (1997) Proton-translocation by membrane-bound NADH: ubiquinone-oxidoreductase (complex I) through redox-gated ligand conduction, *Biochim. Biophys. Acta 1318*, 79−91.
19. Magnitsky, S., Toulokhonova, L., Yano, T., Sled, V. D., Hagerhall, C., Grivennikova, V. G., Burbaev, D. S., Vinogradov, A. D., and Ohnishi, T. (2002) EPR Characterization of Ubisemiquinone and Iron−Sulfur Cluster N2, Central Components of the Energy Coupling in the NADH−Ubiquinone Oxidoreductase (Complex I) In Situ, *J. Bioenerg. Biomembr. 34*, 193−208.
20. Yano, T., Dunham, W. R., and Ohnishi, T. (2005) Characterization of the $\Delta\mu$H+-sensitive ubisemiquinone species (SQNf) and the interaction with cluster N2: New insight into the energy-coupled electron transfer in complex I, *Biochemistry 44*, 1744−1754.
21. Friedrich, T., and Scheide, D. (2000) The respiratory complex I of bacteria, archaea and eukarya and its module common with membrane-bound multisubunit hydrogenases, *FEBS Lett. 479*, 1−5.
22. Brandt, U., Kerscher, S., Dröse, S., Zwicker, K., and Zickermann, V. (2003) Proton pumping by NADH: ubiquinone oxidoreductase. A redox driven conformational change mechanism? *FEBS Lett. 545*, 9−17.
23. Yano, T., and Ohnishi, T. (2001) The origin of cluster N2 of the energy-transducting NADH-quinone oxidoreductase: comparisons of phylogenetically related enzymes, *J. Bioenerg. Biomembr. 33*, 213−221.
24. Ahlers, P. M., Zwicker, K., Kerscher, S., and Brandt, U. (2000) Function of Conserved Acidic Residues in the PSST Homologue of Complex I (NADH: Ubiquinone Oxidoreductase) from *Yarrowia lipolytica*, *J. Biol. Chem. 275*, 23577−23582.
25. Grgic, L., Zwicker, K., Kashani-Poor, N., Kerscher, S., and Brandt, U. (2004) Functional significance of conserved histidines and arginines in the 49-kDa subunit of mitochondrial complex I, *J. Biol. Chem. 279*, 21193-21199.

26. Mäntele, W. (1996) Infrared and Fourier transform infrared spectroscopy, in *Biophysical Techniques in Photosynthesis* (Amesz, J. and Hoff, A. J., Eds.) pp 137−160, Kluwer Academic Publishers, Dordrecht.
27. Zscherp, C., and Barth, A. (2001) Reaction-induced infrared difference spectroscopy for the study of protein reaction mechanisms, *Biochemistry 40*, 1875−1883.
28. Hellwig, P., Scheide, D., Bungert, S., Mäntele, W., and Friedrich, T. (2000) FT-IR spectroscopic characterization of NADH: ubiquinone oxidoreductase (complex I) from *Esherichia coli*: oxidation of FeS cluster N2 is coupled with the protonation of an aspartate or glutamate side chain, *Biochemistry 39*, 10884−10891.
29. Flemming, D., Hellwig, P., and Friedrich, T. (2003) Involvement of Tyrosines 114 and 139 of Subunit NuoB in the Proton Pathway around Cluster N2 in *Escherichia coli* NADH: Ubiquinone Oxidoreductase, *J. Biol. Chem. 278*, 3055−3062.
30. Hellwig, P., Stolpe, S., and Friedrich, T. (2004) Fourier Transform Infrared Spectroscopic Study on the Conformational Reorganisation in *Escherichia coli* Complex I Due to Redox-Driven Proton Translocation, *Biopolymers 74*, 69−72.
31. Goormaghtigh, E., Raussens, V., and Ruysschaert, J.-M. (1999) Attenuated total reflection infrared spectroscopy of proteins and lipids in biological membranes, *Biochim. Biophys. Acta 1422*, 105−185.
32. Rothschild, K. J., Bousche, O., Braiman, M. S., Hasselbacher, C. A., and Spudich, J. L. (1988) Fourier transform infrared study of the halorhodopsin chloride pump, *Biochemistry 27*, 2420−2424.
33. Heberle, J. and Zscherp, C. (1996) ATR/FT-IR difference spectroscopy of biological matter with microsecond time resolution, *Appl. Spectrosc. 50*, 588−596.
34. Rich, P. R., and Iwaki, M. (2005) Infrared Protein Spectroscopy as a Tool to Study Protonation Reactions Within Proteins, in *Biophysical and Structural Aspects of Bioenergetics* (Wikström, M., Ed.) pp 314−333, Royal Society of Chemistry, Cambridge, U.K.
35. Kerscher, S., Dröse, S., Zwicker, K., Zickermann, V., and Brandt, U. (2002) *Yarrowia lipolytica*, a yeast genetic system to study mitochondrial complex I, *Biochim. Biophys. Acta 1555*, 83−91.
36. Sharpley, M. S., Shannon, R. J., Draghi, F., and Hirst, J. (2005) Interactions between phospholipids and NADH: ubiquinone oxidoreductase (complex I) from bovine mitochondria, *Biochemistry 45*, 241−248.
37. Plesnicar, M., and Bendall, D. S. (1970) The plastocyanin content of chloroplasts from some higher plants estimated by a sensitive enzymatic assay, *Biochim. Biophys. Acta 216*, 192−199.
38. DeGrip, W. J., Gray, D., Gillespie, J., Bovee, P. H. M., Van den Berg, E. M. M., Lugtenberg, J., and Rothschild, K. J. (1988) Photoexcitation of rhodopsin: conformation changes in the chromophore, protein and associated lipids as determined by FTIR difference spectroscopy, *Photobiochem. Photobiophys. 48*, 497−504.
39. Glasoe, P. K. and Long, F. A. (1960) Use of glass electrodes to measure acidities in deuterium oxide, *J. Phys. Chem. 64*, 188−190.
40. Rath, P., DeGrip, W. J., and Rothschild, K. J. (1998) Photoactivation of rhodopsin causes an increased hydrogen−deuterium exchange of buried peptide groups, *Biophys. J. 74*, 192−198.
41. Iwaki, M., Yakovlev, G., Hirst, J., Osyczka, A., Dutton, P. L., Marshall, D., and Rich, P. R. (2005) Direct observation of redox-linked histidine protonation changes in the iron−sulfur protein of cytochrome bc_1 complex by ATR-FTIR spectroscopy, *Biochemistry 44*, 4230−4237.
42. Wille, G., Ritter, M., Friedemann, R., Mäntele, W., and Hübner, G. (2003) Redox-triggered FTIR difference spectra of FAD in aqueous solution and bound to flavoproteins, *Biochemistry 42*, 14814−14821.
43. Sery, A., Housset, D., Serre, L., Bonicel, J., Hatchikian, C., Frey, M., and Roth, M. (1994) Crystal structure of the ferredoxin I from *Desulfovibrio africanus* at 2.3 Å resolution, *Biochemistry 33*, 15408−15417.
44. Davy, S. D., Osborne, M. J., and Moore, G. R. (1998) Determination of the structure of oxidised *Desulfovibrio africanus* ferredoxin I by ^{1}H NMR spectroscopy and comparison of its solution structure with its crystal structure, *J. Mol. Biol. 277*, 683−706.
45. Echols, N., Milburn, D., and Gerstein, M. (2003) MolMovDB: analysis and visualization of conformational change and structural flexibility, *Nucleic Acids Res. 31*, 478−482.
46. Dröse, S., Zwicker, K., and Brandt, U. (2002) Full recovery of the NADH: ubiquinone activity of complex I (NADH: ubiquinone oxidoreductase) from *Yarrowia lipolytica* by the addition of phospholipids, *Biochim. Biophys. Acta 1556*, 65−72.
47. Dröse, S., Galkin, A., and Brandt, U. (2005) Proton pumping by complex I (NADH: ubiquinone oxidoreductase) from *Yarrowia lipolytica* reconstituted into proteoliposomes, *Biochim. Biophys. Acta 1710*, 87−95.
48. Nakashima, Y., Shinzawa-Itoh, K., Watanabe, K., Naoki, K., Hano, N., and Yoshikawa, S. (2002) Steady-State Kinetics of NADH: coenzyme Q oxidoreductase Isolated from Bovine Heart Mitochondria, *J. Bioenerg. Biomembr. 34*, 11−19.
49. Carroll, J., Shannon, R. J., Fearnley, I. M., Walker, J. E., and Hirst, J. (2002) Definition of the nuclear encoded protein composition of bovine heart mitochondrial complex I, *J. Biol. Chem. 277*, 50311−50317.
50. Burie, J.-R., Boussac, A., Boullais, C., Berger, G., Mattioli, T., Mioskowski, C., Nabedryk, E., and Breton, J. (1995) FTIR spectroscopy of UV-generated quinone radicals: Evidence for an intramolecular hydrogen atom transfer in ubiquinone, naphthoquinone, and plastoquinone, *J. Phys. Chem. 99*, 4059−4070.
51. Bauscher, M., Nabedryk, E., Bagley, K., Breton, J., and Mäntele, W. (1990) Investigation of models for photosynthetic electron acceptors: Infrared spectroelectrochemistry of ubiquinone and its anions, *FEBS Lett. 261*, 191−195.
52. Bauscher, M., and Mäntele, W. (1992) Electrochemical and infrared-spectroscopic characterization of redox reactions of p-quinones, *J. Phys. Chem. 96*, 11101−11108.
53. Hellwig, P., Mogi, T., Tomson, F. L., Gennis, R. B., Iwata, J., Miyoshi, H., and Mäntele, W. (1999) Vibrational modes of ubiquinone in cytochrome bo_3 from *Escherichia coli* identified by Fourier transform infrared difference spectroscopy and specific ^{13}C labeling, *Biochemistry 38*, 14683−14689.
54. Ritter, M., Anderka, O., Ludwig, B., Mäntele, W., and Hellwig, P. (2003) Electrochemical and FTIR spectroscopic characterization of the cytochrome bc_1 complex from *Paracoccus denitrificans*: Evidence for protonation reactions coupled to quinone binding, *Biochemistry 42*, 12391−12399.
55. Iwaki, M., Osyczka, A., Moser, C. C., Dutton, P. L., and Rich, P. R. (2004) ATR-FTIR spectroscopy studies of ion-sulfur protein and cytochrome c_1 in the *Rhodobacter capsulatus* cytochrome bc_1 complex, *Biochemistry 43*, 9477−9486.
56. Breton, J., Burie, J.-R., Berthomieu, C., Berger, G., and Nabedryk, E. (1994) The binding sites of quinones in photosynthetic bacterial reaction centers investigated by light-induced FTIR difference spectroscopy: Assignment of the Q_A vibrations in *Rhodobacter sphaeroides* using ^{18}O− or ^{13}C-labeled ubiquinone and vitamin K_1, *Biochemistry 33*, 4953−4965.
57. Clark, W. M. (1960) *Oxidation−reduction potentials of organic systems*, Bailliere, Tindall & Cox, Ltd., London.
58. Kerscher, S., Zickermann, V., Zwicker, K., and Brandt, U. (2005) Insights into the mechanism of mitchondrial complex I from its distant relatives, the [NiFe] hydrogenases, in *Biophysical and Structural Aspects of Bioenergetics* (Wikström, M., Ed.) pp 156−184, Royal Society of Chemistry, Cambridge, U.K.
59. Venyaminov, S. Y., and Kalnin, N. N. (1990) Quantitative IR spectrophotometry of peptide compounds in water (H_2O) solutions. I. Spectral parameters of amino acid residue absorption bands, *Biopolymers 30*, 1243−1257.
60. Barth, A. (2000) The infrared absorption of amino acid side chains, *Prog. Biophys. Mol. Biol. 74*, 141−173.
61. Barth, A., and Zscherp, C. (2002) What vibrations tell us about proteins, *Q. Rev. Biophys. 35*, 369−430.
62. Haris, P. I., Robillard, G. T., van Dijk, A. A., and Chapman, D. (1992) Potential of ^{13}C and ^{15}N labeling for studying protein−protein interactions using Fourier transform infrared spectroscopy, *Biochemistry 31*, 6279−6284.
63. Xiao, Y., Hutson, M. S., Belenky, M., Herzfeld, J., and Braiman, M. S. (2004) Role of arginine-82 in fast proton release during the bacteriorhodopsin photocycle: a time-resolved FT-IR study of purple membranes containing ^{15}N labeled arginine, *Biochemistry 43*, 12809−12818.
64. Noguchi, T., Inoue, Y., and Tang, X.-S. (1999) Structure of a histidine ligand in the photosynthetic oxygen-evolving complex as studied by light-induced Fourier transform infrared difference spectroscopy, *Biochemistry 38*, 10187−10195.

65. Hasegawa, K., Ono, T.-A., and Noguchi, T. (2002) Ab initio density functional theory calculations and vibrational analysis of zinc-bound 4-methilimidazole as a model of a histidine ligand in metalloenzymes, *J. Phys. Chem. A 106*, 3377−3390.
66. Hasegawa, K., Ono, T.-A., and Noguchi, T. (2000) Vibrational spectra and Ab Initio DFT calculations of 4-methylimidazole and its different protonation forms: Infrared and Raman markers of the protonation state of a histidine side chain, *J. Phys. Chem. B 104*, 4253−4265.
67. Berthomieu, C., Boullais, C., Neumann, J.-M., and Boussac, A. (1998) Effect of ^{13}C, ^{18}O- and ^{2}H-labeling on the infrared modes of UV-induced phenoxyl radicals, *Biochim. Biophys. Acta 1365*, 112−116.
68. Hienerwadel, R., Boussac, A., Breton, J., and Berthomieu, C. (1997) Fourier transform infrared difference spectroscopy of photosystem II tyrosine D using site-directed mutagenesis and specific isotope labeling, *Biochemistry 36*, 14712−14723.
69. Hellwig, P., Pfitzner, U., Behr, J., Rost, B., Pesavento, P., Donk, W. v., Gennis, R. B., Michel, H., Ludwig, B., and Mäntele, W. (2002) Vibrational modes of tyrosine in cytochrome *c* oxidase from *Paracoccus* denitrificans: FTIR and electrochemical studies on Tyr-D4-labeled and on Tyr280His and Tyr35Phe mutant enzymes, *Biochemistry 41*, 9116−9125.

BI052561E